
Design and Performance of Posicam 6.5 BGO Positron Camera

N.A. Mullani, K. Lance Gould, R.K. Hartz, R.E. Hitchens, W.H. Wong, D. Bristow, S. Adler, E.A. Philippe, B. Bendriem, M. Sanders, and B. Gibbs

Positron Diagnostic and Research Center, The University of Texas Health Science Center at Houston, Texas; Positron Corporation, Houston, Texas; and Brookhaven National Labs, Upton, New York

A high-resolution, whole-body positron camera, POSICAM 6.5 BGO, has been designed, built, and tested; results from it are presented. The camera utilizes 1,320 BGO crystals and 720 PMTS in a staggered geometry to produce high resolution of 5.8 mm FWHM and 21 image planes simultaneously. The axial resolution of the camera is measured at 11.9 mm at the center. High axial sampling is achieved with 5.125 mm separation of the image planes such that three-dimensional imaging of an object can be carried out in a single scan. Recovery of volumetric distribution of radioactivity and object dimensions in axial and sagittal views is demonstrated by imaging spherical objects 13 mm to 39 mm in diameter.

J Nucl Med 1990; 31:610-616

As positron emission tomography (PET) is used more extensively for in vivo quantitation of regional perfusion and metabolism, better PET camera design is needed for more accurate volumetric data recovery. Consequently, fine axial sampling is essential in addition to in plane sampling in order to produce three-dimensional imaging for systems based on multiple two-dimensional image-planes.

The importance of finer axial sampling for three-dimensional imaging of the heart, and greater diagnostic accuracy, has been demonstrated by Senda et al. (1) in both phantoms and patient studies. They showed increased sensitivity of detecting myocardial perfusion defects by incorporating a second scan of the heart obtained by moving the patient one-half the image plane separation. Specificity also improved due to the finer axial sampling provided by the second interleaved scan, thereby avoiding artifactual false-positive results. In our own clinical experience with three-dimensional imaging of the heart with TOFPET I (2), even with close spacing of image planes (10.8 mm separation for 11 mm axial resolution), movement of the patient or

detector and a second scan is required to achieve the necessary axial sampling for volumetric data recovery (3). Movement of either patient or detectors creates several problems, especially with short-lived isotopes. Data are lost during the time required for the movement and interleaved image planes taken at a later time contain different physiologic data. For short half-life radionuclides, such as rubidium-82 (^{82}Rb) and oxygen-15 (^{15}O), a second scan cannot be obtained without injecting the radionuclides a second time. During the time required to obtain adequate counts on the first scan, activity decays sufficiently to prevent acquisition of a second scan. These limitations hinder three-dimensional quantitation of the physiologic process with very short-lived radionuclides, unless a PET camera with high axial sampling is used.

The POSICAM camera had the following design goals to overcome problems of data loss and activity decay:

1. Three-dimensional volumetric imaging with a single scan.
2. Fast imaging with high count rate capability for short-lived isotopes such as ^{82}Rb and ^{15}O .
3. High resolution for the heart (whole body) and brain.

To reach these goals, a new detector design was developed and patented (4). Every other detector in each ring is staggered by one-half position to achieve the same spatial sampling frequency as moving the detectors in the axial direction for an interleaved slice. When compared to conventional detector geometry without staggering, the staggered design halves the sampling distance in the axial direction, and almost doubles the number of slices collected simultaneously by the camera. The detector design also allows shorter septa, which in turn allows a smaller, more compact mechanical gantry. The detector design uses conventional $\frac{3}{4}$ " photomultiplier tubes (PMT) and a conservative 2:1 crystal to PMT positioning scheme in order to minimize specialized electronics and simplify the encoding scheme for more stable operation. The system has been designed to accept a variety of different scintillators, including barium fluoride (BaF_2) (5) and bismuth ger-

Received May 17, 1989; revision accepted Dec. 21, 1989.
For reprints contact: Nizar Mullani, Division of Cardiology, University of Texas Medical School, 6431 Fannin, Houston, TX 77030.

minate (BGO) (6). A time-of-flight (TOF) option can also be added to the BaF₂ system with little change in the detectors and gantry designs. This paper describes preliminary performance of the POSICAM 6.5 having six rings of BGO detectors (five staggered rings) simultaneously producing 21 overlapping image planes.

CAMERA DESIGN

A drawing of the POSICAM camera is shown in Figure 1. A brief description of certain elements of the camera is included.

The donut-shaped assembly for holding the detectors is made of half-inch steel for structural support and shielding against scattered radiation. The detectors and septa are mounted on a moving plate inside this structure, which move eccentrically (wobble) with a diameter of 22 mm for better sampling during the scan (7). The septa are donut-shaped and are made of 1.5 mm thick lead, 7 cm long. They are attached to the detector module plate and wobble with the detectors as a unit. Lead shielding, varying from 5 to 7 cm in thickness, is attached to the stationary part of the gantry to minimize the scattered radiation reaching the detectors from the patient's body outside of the axial field of view. The design of the septa is essentially dictated by the compromise between accepted randoms, scatter events, and sensitivity for true counts (8,9).

The POSICAM 6.5 BGO camera utilizes 1,320 BGO

scintillation crystals 8.5×20×30 mm in size. These crystals are viewed by 720 PMTs, which detect the scintillation light and convert it to electrical pulses. The detectors and PMTs are grouped in 120 modules, each with 11 crystals and 6 PMTs that are placed in a circle with a diameter of 78 cm. Each module of 11 crystals and 6 PMTs is light-tight and self-contained. The modules are placed radially around the circle such that the six PMTs are aligned with the axial direction of the gantry.

The staggered detector design doubles the axial sampling and the number of slices, while reducing the slice separation to 5.125 mm. Every alternate detector in the circle of crystals is offset by one-half the detector position, axially. The offset produces axial sampling which is equivalent to manually moving the detectors by one-quarter of the detector length.

The placement of PMTs and crystals is shown in Figure 2. The crystals are numbered 1 through 11 and the PMTs are labeled A through F. Light output from crystal 1 is collected mostly by PMT A, and similarly, the light output from crystal 3 is collected mostly by PMT B. The light from crystal 2 is shared equally between PMT A and PMT B. The system for collecting light from 11 crystals to 6 PMTs is referred to as a 2:1 system because of two-to-one splitting of light for encoding. The 2:1 detector positioning is easily encoded and decoded since there is a large difference in the signals between the two PMTs for the three crystal positions. The large separation of the PMT outputs for crystal identification also permits greater variation of PMT performance without significantly affecting detector encoding accuracy.

POSICAM GANTRY FEATURES

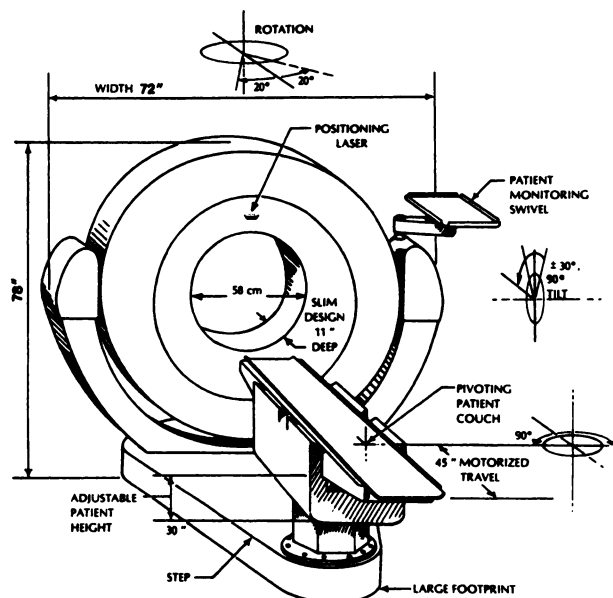


FIGURE 1
Artist's drawing of the POSICAM mechanical gantry. Several features of the system such as rotation, tilt, and patient couch rotation are illustrated in the drawing. A large footprint of the base distributes the weight over a large area for easy installation with few on-site structural changes.

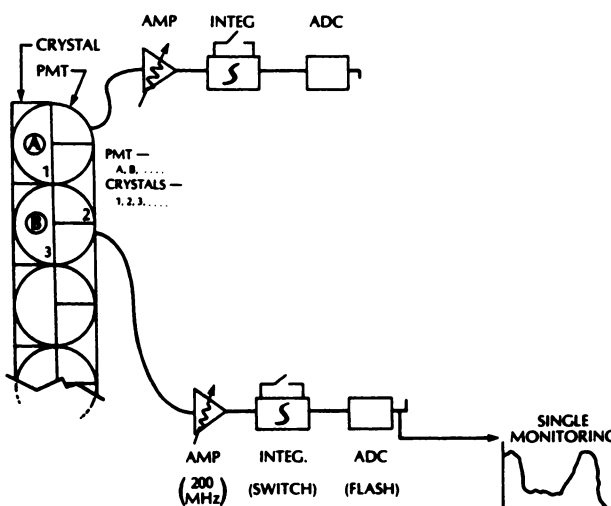


FIGURE 2
A plan drawing of the crystals and PMT arrangement for the POSICAM detector module. The crystals are numbered 1 through 11 and the PMTs are labeled A through F. Light output from crystal 1 is primarily detected by PMT A, while light output from crystal 2 is detected by PMTs A and B equally.

Data acquisition and image processing are handled by a multiprocessor system comprised of two VME-based systems and a VAX computer. The VME-based systems allow simultaneous operation of data acquisition and image reconstruction while the VAX functions as the host and image processing system. The data acquisition system is capable of operating at ~1 million cps in the binned profile mode or list mode of data collection (2).

METHODS

The POSICAM 6.5 BGO system has been tested for preliminary results and the camera design has been simulated with the Geant III Monte Carlo code from CERN (10). The testing and simulation covers several aspects of the camera (including resolution and sensitivity) for performance comparison with theoretically possible performance. The following tests were carried out on the POSICAM camera to evaluate its overall performance.

Resolution

A single 1 mm in diameter germanium-68 line source positron source encased in a steel tube with an approximate outside diameter of 2 mm was scanned at three different locations from the center, i.e. at radial position of $r = 0$, $r = 10$, and $r = 20$ cm. The point source was scanned in air at a high count rate of ~250,000 cps. Radial and tangential measurements of resolutions were obtained from the reconstructed images by taking profiles through the images and fitting Gaussian profiles to the data.

Fluorine-18 sources ~2 mm in diameter were used to measure axial resolution. The sources were attached to the patient pallet and, under computer control, these sources were scanned at many different axial locations stepped in increments of 2 mm. A region of interest (ROI) was drawn around the point source in the image plane. A profile of axial response function was obtained from several scan positions. The ROI data was then plotted as a function of patient pallet position and the full width at half maximum (FWHM) value was measured for different slices (assuming a Gaussian distribution in the axial direction). The axial resolution was measured for three different radial positions of the source at $r = 0$, $r = 10$, and $r = 20$ cm from the center.

Sensitivity

The sensitivity of the camera was measured by placing a uniformly distributed source of radioactivity in a cylinder of 20 cm diameter and 19 cm length. The length of the cylinder was arbitrarily chosen in order to cover the 12.3-cm axial field of view. The source was scanned at a low radioactivity concentration of ~0.1 $\mu\text{Ci}/\text{cc}$ where the deadtime losses and randoms are negligible. The energy threshold of the system was typically set at 350 keV and sensitivity was measured as the total number of counts collected by the system, including scatter, after subtraction for randoms.

Scatter

Scatter was measured with a line source in air and in a 20-cm diameter scattering medium. Scatter data were also simulated with the Geant Monte Carlo simulation program and the scatter fraction (defined as the ratio of scatter to true

counts) was estimated from the simulated data by Bendriem et al. (10). A scatter deconvolution filter was derived and applied to the binned profiles before image reconstruction.

A uniform phantom of 20 cm diameter with a 5-cm filling defect also was scanned with the hole positioned at the center as well as off-center for evaluation of the scatter correction algorithm. A ROI was drawn in the 5-cm hole, as well as in the surrounding activity, to assess the amount of scattered radiation and the residual error after subsequent scatter correction.

Randoms

A uniform phantom source, 20 cm in diameter by 19 cm long (5,440 cc), was scanned with high levels of activity in excess of 20 mCi and allowed to decay. Sequential scans were conducted to correlate the activity level to the detected counts. The number of randoms was estimated from the tails of the binned profiles that extend from radial positions of greater than $r = 20$ cm, in order to minimize the amount of scatter in the randoms estimation. Randoms were also calculated from the singles rate measured by the system. The true and random events were recovered from the ROI drawn around the uniform phantom. The true counts and random counts were plotted against known activity levels in the phantom for this large uniform distribution phantom exceeding the axial field of view.

Deadtime Losses

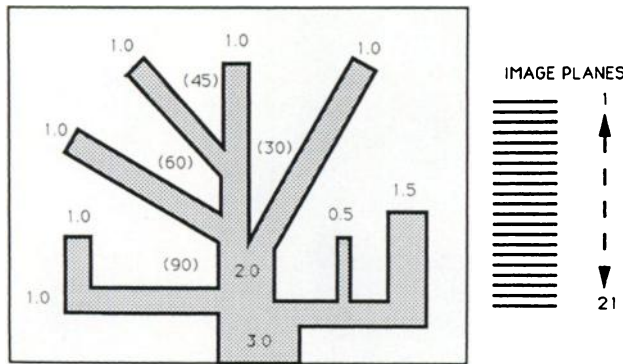
Deadtime losses are an important characteristic of the PET camera since they limit the collection of counts from the patient. These losses are complex enough that they cannot be treated with a single correction factor unless the system is well-characterized (11). There are several areas of deadtime losses: (a) the singles at the module; (b) the encoder and coincidence circuits; and (c) the data transfer. Deadtime losses are measured from the true counts obtained after random subtraction. A 20-cm diameter source filled with a short-lived isotope is scanned several times at different concentrations. True counts are obtained from the data and the expected true counts at high count rates are linearly extrapolated from the low count-rate values to obtain an estimation of deadtime losses.

Axial Sampling

The effect of inadequate axial sampling in both axial directions and the partial volume errors, caused by angulation of an organ with respect to the imaged plane, can be simultaneously demonstrated by a special phantom (12). Several 1-cm thick fingers of radioactivity were placed in the field of view at angles of 0, 30, 45, 60, and 90 degrees to the axial direction. These fingers of radioactivity simulating the myocardium at different positions were scanned with a single scan. The reconstructed images were displayed by creating long axis slices through them such that all the fingers of radioactivity are viewed. The drawing of the phantom is shown in Figure 3. This phantom has been designed to quantitate the recovery coefficients for volumetric imaging as a function of the object size and the angle of the involved plane. Detailed information is presented in a separate publication by Mullani (12).

Resolution Uniformity

In order to evaluate the uniformity of resolution across the 20-cm field of view, the Derenzo (13) phantom was scanned



PARTIAL VOLUME PHANTOM

FIGURE 3

Special partial volume and axial sampling phantom which simulates the myocardium at different angles with respect to the imaged plane. The walls of the myocardium are 1 cm thick and inclined at 0, 30, 45, 60 and 90 degrees. Axial sampling and quantitation errors due to partial volume errors are demonstrated by taking coronal sections through the data.

with a low concentration of radioactivity and reconstructed using the calculated attenuation correction.

Spheres

Three-dimensional volumetric quantitation of POSICAM was tested by scanning, with a single scan, several spheres (14) which are 13, 16, 21, 24, 31, and 39 mm in diameter. The spheres were positioned in a circle of ~5 cm radius and placed in a 20-cm diameter, uniform distribution of attenuating medium such as water. All the spheres were filled with the same concentration of radioactivity.

Profiles were drawn through the spheres in the reconstructed images and the 50% points of the maximum in the profiles were used as edges of the spheres. Sagittal and coronal views also were obtained from all the slices. Regions of interest were drawn over each sphere in each slice and three-dimensional count density was plotted against the known volume of the spheres. The plotted density was used to assess the system's capability of recovering three-dimensional volumetric concentrations with a single scan.

RESULTS

Resolution

The radial and tangential resolutions are shown in Table 1. The resolution predicted by the Monte Carlo

TABLE 1
Radial, Tangential, and Axial Resolutions Measured with a Point Source in Air at Three Different Positions in the Field of View

	Resolution in mm		
	FWHM		
	r = 0	r = 10	r = 20
Radial	5.8	6.3	7.9
Tangential	5.8	6.3	6.3
Axial (average)	11.9	12.8	14.3

simulation of the POSICAM 6.5 BGO is 5.5 mm FWHM at the center while the measured resolution is 5.8 mm FWHM. The average axial resolution for all slices was measured at 11.9 mm FWHM at the center. The average axial resolution at r = 10 cm was 12.8 mm FWHM; r = 20 was 14.1 mm FWHM. Within a 20-cm diameter region, the radial, tangential, and axial resolutions changed <10% from those values at the center. For a 40-cm diameter object, there was <20% changes in the tangential and axial resolutions but a 36% change in radial resolution.

Sensitivity

The measured sensitivity was ~180,000 cps/μCi/cc, for an energy setting of ~350 keV. Table 2 lists the relative sensitivity of each image plane and the variation in sensitivity from slice to slice. The variation in the sensitivity from slice to slice was found to be < ±13% of the average sensitivity for the 17 inner slices.

Scatter

The percent of scatter in an image was estimated by scanning a line source in air and in a scattering medium of 20 cm in diameter. The scatter data was then deconvolved from out of the binned profile data using the deconvolution method described previously (10). An experimental estimate from this technique which accurately corrects for scatter is 18% of the total data for the 20-cm uniform phantom. Monte Carlo simulation of scatter ranged from 18% to 24%, depending on the energy threshold settings. Scatter correction for the POSICAM 6.5 also was demonstrated using the 20-cm diameter source with a 5-cm defect in the center. A residual error of <2% was seen in the hole following the scatter correction.

Randoms

The relationship between randoms and trues as a function of the total radioactivity in the field of view is shown in Figure 4. The concentration at which randoms equaled trues was 2.4 μCi/cc and the total activity in

TABLE 2
Relative Sensitivity of each Slice as Measured with a 20-cm Diameter Uniform Phantom with Starting Activity Levels of Approximately 1 μCi/cc

Slice	Relative sensitivity	Slice	Relative sensitivity
1	0.32	12	1.05
2	0.50	13	1.25
3	0.79	14	1.05
4	0.95	15	1.19
5	1.17	16	1.02
6	0.96	17	1.17
7	1.14	18	0.95
8	1.02	19	0.75
9	1.21	20	0.48
10	1.01	21	0.27
11	1.19	—	—

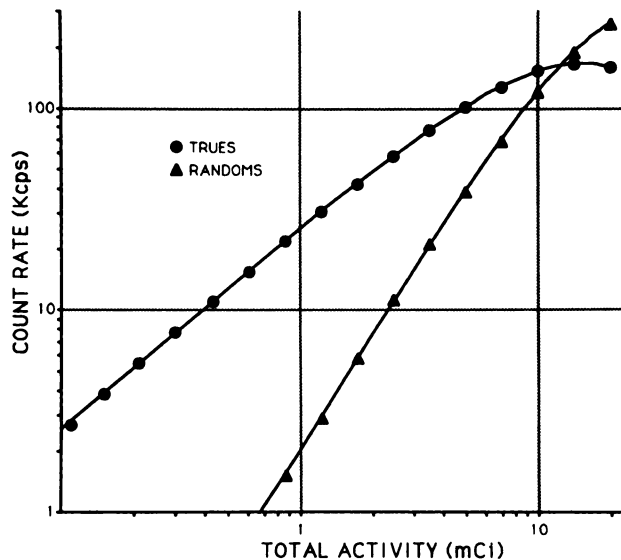


FIGURE 4
The relationship between trues and randoms counts as detected by POSICAM in a 20-cm diameter uniform source 19 cm deep as a function of the total activity in the phantom.

the 20 cm diameter by 19 cm long phantom was 13 mCi. The ratio of total singles in the system to the true counts measured at low count rates is ~ 38 . In other words, $\sim 2.8\%$ of the total activity detected by the detectors results in true coincidences.

Deadtime Losses

Deadtime loss for the POSICAM 6.5 BGO system was demonstrated by monitoring the count rates at several concentration levels using a short-lived source. The data is plotted in Figure 4 for decaying radioactivity in the 20-cm diameter uniform phantom. Randoms were measured at the edges of the profiles and the total counts collected from the 20-cm region are broken down into trues and randoms. The point at which 50% of the trues are lost due to deadtime occurs with 12 mCi in the phantom.

Axial Sampling

The axial sampling capability of POSICAM was demonstrated by scanning the special phantom which simulates myocardial activity at 0, 30, 45, and 60 degree angles to the image plane, as shown in Figure 3. All 21 slices are collected simultaneously in a single scan, with long axis views subsequently obtained from these images (Fig. 5). The simulated myocardial activity at all angles were recovered uniformly because the POSICAM system has sufficient axial sampling with respect to its axial resolution. No sampling artifacts are observed in the images.

Resolution Uniformity

The resolution capability of the system and uniform response within the 20-cm field of view were demonstrated with the Derenzo phantom (13) as shown in

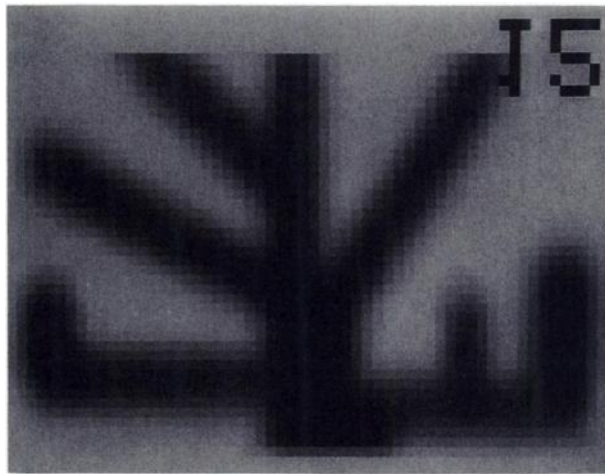


FIGURE 5
Axial view obtained from the 21 slices of the axial sampling phantom show the uniform recovery of myocardial activity regardless of the tilt angle with respect to the image plane.

Figure 6. Fifty million counts were collected in the phantom. The image was reconstructed using the ramp filter.

Imaging of Spheres

Spheres of 13, 16, 21, 24, 33, and 39 mm diameter were filled with uniform activity and placed in scattering medium consisting of a 20-cm diameter phantom. Axial views of the spheres obtained through two spheres at a time (Fig. 7) show the ability of POSICAM system to recover three-dimensional activity distribution.

Regions of interest were drawn in all the slices for the six spheres, and activities in these ROIs for the different slices were summed together to form a three-dimensional ROI over the sphere. PET counts measured with these three-dimensional ROIs were then compared with the volumes of the spheres and shows the

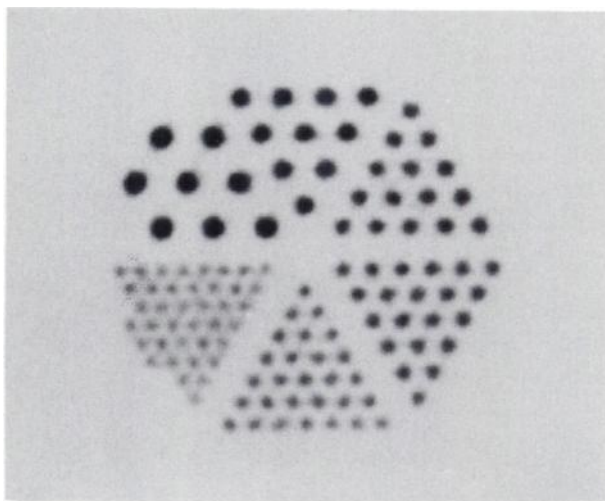


FIGURE 6
Derenzo phantom reconstructed with the ramp filter. The image contains ~ 50 million counts.

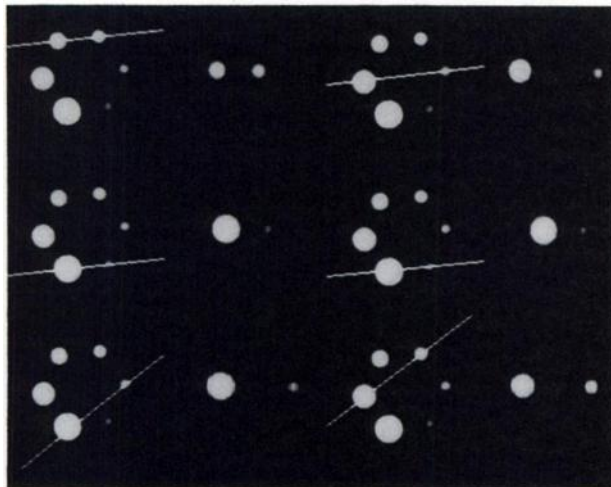


FIGURE 7
Axial cuts (sagittal & coronal views) through the spheres are shown for different angles and spheres next to the transaxial image. The spheres are 13, 16, 21, 24, 31 and 39 mm in diameter. The line through the spheres shows the plane of the axial cut and the resulting image produced along this plane is shown to the right of the transaxial image.

recovery of the volumetric information from 1.3 cc to 39 cc sized objects (Fig. 8).

Profiles were also drawn through the spheres in the transaxial planes and in the axial direction. The 50% level of the maximum amplitude of each was then used

**JORDAN SPHERES VOLUME MEASUREMENT
POSICAM 6.5 BGO**

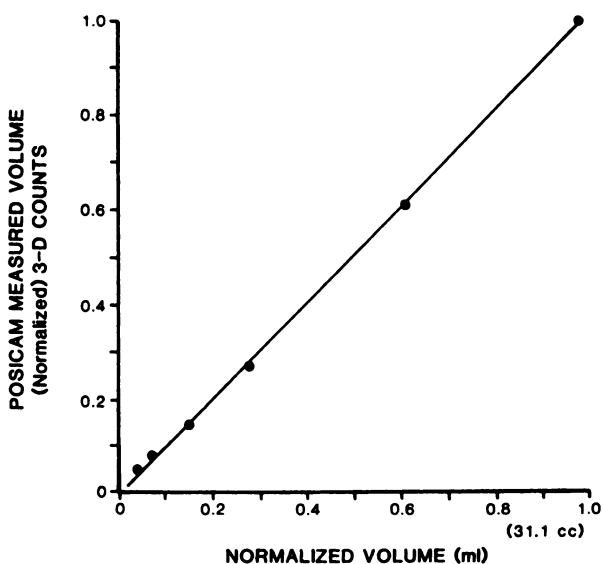


FIGURE 8
Total counts measured in the 3-D ROI for the spheres are plotted against the known volumes of the sphere. The relationship is linear except for the smallest sphere of 1.3 cc where the PET measured activity is overestimated partly due to partial volume effects.

**3D MEASUREMENT OF OBJECT DIMENSIONS
BY POSICAM 6.5 BGO**

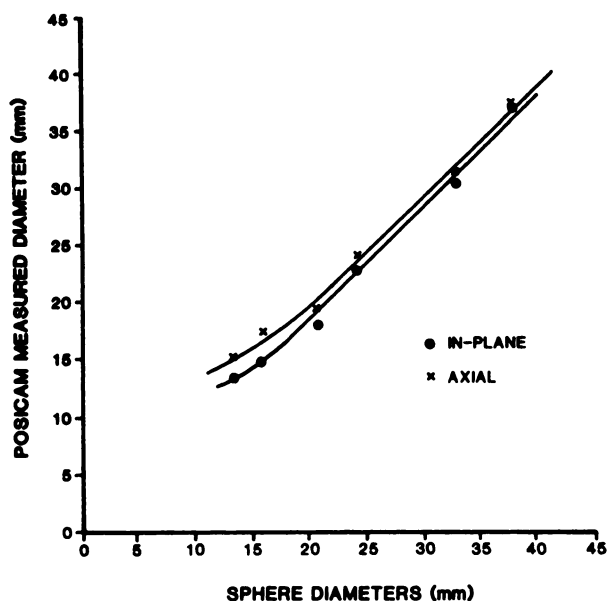


FIGURE 9
Diameter of the spheres measured in-plane and in the axial direction plotted against the known diameters of the spheres. Data was obtained from a single scan of the spheres phantom.

to measure the diameter of the spheres, which were plotted as a function of the true diameters of the spheres (Fig. 9).

Heart Phantom

The heart phantom from Data Spectrum (Chapel Hill, NC) was imaged with radioactivity in the myocardium which included a defect of 1 cm by 2 cm. There was a low background level of ventricular activity surrounding the myocardium. The 21 slices obtained from the heart phantom are shown in Figure 10.

CONCLUSION

This multi-slice system is designed for fast three-dimensional volumetric imaging with a single scan. The results demonstrate accurate recovery of activity concentrations and dimensions for objects which are 16 mm or greater.

The high resolution capability of the system and its uniformity of resolution across the field of view have been shown. Variation in sensitivity of adjacent image planes also has been demonstrated to be quite small. This uniformity of sensitivity makes the signal-to-noise characteristics of the data comparable from one slice to the other.

ACKNOWLEDGMENTS

The authors wish to thank Ro Edens, Claire Finn, Kathy Norred, and Kathy Rainbird in preparing the manuscript. The

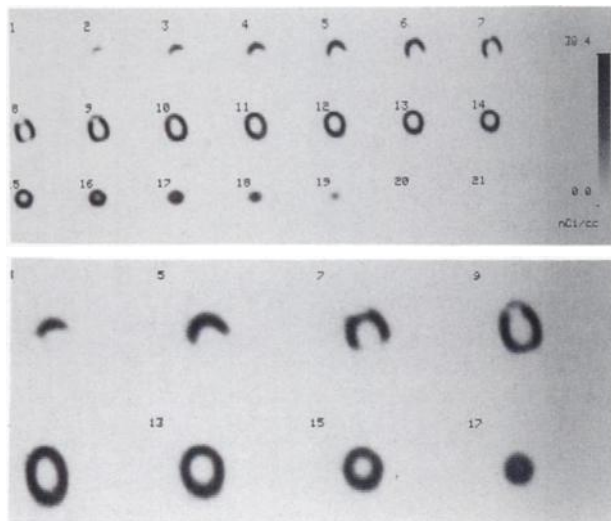


FIGURE 10
Transaxial slices of the Data Spectrum Heart phantom. Twenty-one slices are collected simultaneously and a few selected slices are enlarged in the lower part of the display. A 1 cm × 2 cm defect is clearly seen in several slices.

authors also thank the Department of Nuclear Medicine at the National Institute of Health for its scientific contributions and the production of radioactivity. We also thank Professor Jordan and Dr. Knopp at Hanover for the use of their phantoms.

This research was carried out in part as a joint collaborative effort with the Clayton Foundation for Research, and was funded in part by DOE grant DE-FG05-84ER60210 and NIH grants RO1-H1-26862 and RO1-HL26855.

Presented in parts at the European Society of Nuclear Medicine meeting, London, August 1985, and The Society of Nuclear Medicine meeting, June 1986, Washington, DC.

REFERENCES

1. Senda M, Yonekura Y, Tamaki N, et al. Interpolating scan and oblique-angle tomograms in myocardial PET using nitrogen-13 ammonia. *J Nucl Med* 1986; 27:830-836.
2. Mullani NA, Gaeta J, Yerial K, et al. Dynamic imaging with high resolution time-of-flight PET camera TOFPET I. *IEEE Trans Nucl Sci* 1984; NS-31:609-613.
3. Mullani NA. The need for three-dimensional imaging in PET. *Proceedings of the international symposium on current and future aspects of cancer diagnosis with positron emission tomography*. Tohoku, Japan, 1985:228-296.
4. Mullani NA. U.S. Patent Number 4,563,582 Positron Emission Tomography Camera.
5. Wong WH, Mullani NA, Wardworth G, et al. Characteristics of small barium fluoride (BaF₂) scintillator for high resolution time-of-flight positron emission tomography. *IEEE Trans Nucl Sci* 1984; NS-31:381-386.
6. Cho Z, Farukhi MR. Bismuth germanate as a potential scintillation detector in positron cameras. *J Nucl Med* 1977; 18:840-847.
7. Mullani NA, TerPogossian MM, Higgins CS, et al. Engineering aspects of PETT V. *IEEE Trans Nucl Sci* 1979; 26:2703-2705.
8. Derenzo SE. Method for optimizing side shielding in positron emission tomography and for comparing detector materials. *J Nucl Med* 1980; 21:971-977.
9. Mullani NA, Wong WH, Hartz RK, et al. Sensitivity improvement of TOFPET by the utilization of the inter-slice coincidence. *IEEE Trans Nucl Sci* 1982; 29:479-483.
10. Bendriem B, Wong WH, Mullani NA, et al. Analysis of scatter deconvolution technique in conventional PET using Monte Carlo simulation. *J Nucl Med* 1987; 28:681.
11. Thompson CJ, Meyer E. The effect of live time in components of a positron tomography on image quantification. *IEEE Trans Nucl Sci* 1987; 34:337-343.
12. Mullani NA. A phantom for quantitation of partial volume effects in ECT. *IEEE Trans Nucl Sci* 1989; 36:983-987.
13. Derenzo SE, Budinger TF, Muesman RH, et al. Imaging properties of a positron tomography with 280 BGO crystals. *IEEE Trans Nucl Sci* 1981; 28:81-89.